Clean Technologies and Recycling

Clean Technologies and Recycling, 2(4): 170–198.
DOI: 10.3934/ctr.2022010
Received: 06 August 2022
Accepted: 30 September 2022
Published: 13 October 2022

http://www.aimspress.com/journal/ctr

Research article

Design of a hybrid high-throughput fused deposition modeling system for circular economy applications

Tanay Kuclourya, Roberto Monroy, Miguel Castillo, David Baca and Rafiq Ahmad*

Laboratory of Intelligent Manufacturing, Design and Automation (LIMDA), Department of Mechanical Engineering, University of Alberta, 9211 116 Street, Edmonton, AB T6G 1H9, Canada

* **Correspondence:** Email: rafiq.ahmad@ualberta.ca

Abstract: In recent years, recycling of plastics has opened several doors of advancements in the field of additive manufacturing (AM). The process of fused deposition modelling (FDM) has already been utilized for reprocessing waste plastics into filaments and finally printing them into useful products. Yet another concept of extrusion additive manufacturing (EAM) is gaining lots of attention. In this work, a screw assisted system based on EAM is designed and installed alongside a pre-existing FDM system. This system is referred to as the direct FDM (DFDM) system throughout this work. The DFDM system used operates with a 1.75 mm nozzle and has the ability of giving a high throughput. The focus of this work is to use this hybrid system (combination of FDM and DFDM systems) to print both virgin as well as recycled plastics. The scope of this work is to use one technology (either FDM or DFDM) at a time and to use both simultaneously for multi-material printing in future. After several trials of printing and setting up some printing parameters, the proposed system has been able to print with virgin as well as recycled PLA.

Keywords: AM; FDM; EAM; DFDM; throughput; hybrid; PLA

1. Introduction

The plastic recycling process has been facing some challenges such as high transportation and collection costs of waste plastics as well as the low value of recycled content [1]. This has limited the execution of this much-required process to the extent that the plastic recycling rate has been estimated to be only around 9% [2]. Hence, there is a need to compensate for these constraining factors in the long run. DRAM again comes into the picture as it is an economically viable approach to plastic

recycling. It utilizes local plastic wastes for 3D printing [3]. This approach has ultimately resulted in an inclination of material extrusion AM technologies towards the use of recycled plastics to ensure reduced costs and a low carbon footprint [4]. Many polymers, when recycled, still have mechanical properties in the range of their virgin counterpart [5]. Hence, material extrusion AM technologies such as fused deposition modelling (FDM) and direct-FDM (DFDM) technologies [6] aim toward recycled materials to promote zero waste manufacturing. While FDM technology uses filament for layer-by-layer material deposition, DFDM technology directly uses shredded or pelletized plastics for 3D printing [6]. These concepts of DRAM save approximately 130 million kJ of energy per ton of plastic getting recycled [7].

However, AM has been considered a slow manufacturing process when compared to conventional manufacturing technologies [8]. The lack of available materials for 3D printing an object, the type of extrusion heads to print any specific plastic material, the limited speed, printing parameters, control, performance, and building volume in existing machines, and the high cost of materials are some of the downsides that this emerging technology is still facing and that discourages the industry from implementing it into their manufacturing processes [9]. In addition, multi-materials parts design is another insufficiently explored field where several configurations have been analyzed, and multiple gaps exist to make components of this process with multiple materials optimal and more competitive [10]. Different AM processes have different mechanisms and have their own limitations. For instance, some polymers are not readily available in filaments, which restricts their use as an ideal printing material in the FDM process [11]. The extra step of heating causes the filament formation usually unfavorable for these materials. Hence they are most suitable for the direct extrusion process or DFDM process [11]. Many commercial DFDM systems work on extrusion additive manufacturing (EAM). These systems contain screw-based print heads, which have an auger screw that helps transport the molten material [6]. These print heads also have a screw having either a decreasing pitch or a decreasing channel depth or both, which leads to efficient polymer plastification and mixing [12]. Since these systems can be directly fed with shredded or pelletized materials, EAM is emerging as an enabling technology that expands the range of 3D printing materials as these are no more restricted by their mechanical properties in the filament form or by their performance in the filament extrusion process or even by the tolerance requirements [13]. EAM also reduces feedstock fabrication costs and increases the rate of material deposition when compared to the traditional FDM process [11]. However, although DFDM systems do not need filaments and work directly with pellets or shredded plastics, it is always a challenge to ensure uniform extrusion while using plastic feedstock of irregular shape and size [14].

As per the literature, there have been several proposals of screw extrusion designs and several modifications as well as revisions have been done and are still done on the existing designs to make the process more efficient [15–17]. For instance, to eliminate the feeding problems, Reddy included a separate granule feeding unity and a screw having variable channel depth and pitch [18]. A conical crew has also been designed to enhance plastification and material homogenization over a short length [19]. A successful attempt has also been made to adjust the design in order to achieve a better volumetric rate of the extrusion flow [20]. In yet another interesting study, the deposition surface was attached to a robotic arm having movement in six different axes and had a fixed printhead [21]. Another study on Gigabot X, which is a large-scale direct deposition 3D printer, uses FPF (fused particle fabrication) technology for 3D printing. The system was able to print the material at a speed of

6.5× to 13× faster than the conventional 3D printers while maintaining nearly the same mechanical properties [22].

Since hybrid 3D printers are not very popular but are at an evolving phase in the current time, the design of the system in this work aims toward the development of a novel approach for 3D printing by utilizing the benefits of both FDM and DFDM systems. This makes the system hybrid and suitable for multicomponent as well as multi-material printing of a broad range of thermoplastic materials, where the latter is one of the future objectives of this work. The entire system proposed is designed on the basis of extrusion theory and includes features such as cooling, temperature control, and speed control [23] and aims toward high throughput. The system's capabilities will also employ raw materials from 3D printed waste parts and other conventional plastic manufacturing processes. Furthermore, in terms of the environmental problems generated by plastic waste, the system promotes the "Circular Economy" strategy for part production where material after life-use can be easily reincorporated into the supply chain to avoid plastic accumulation.

2. The system design

In this proposed hybrid system, the design of the screw extruder unit was a big challenge. The thermoplastic polymer granules are fed into the hopper, which ensures a controlled and correct feeding rate of material quantity [23]. The feed material is then transported from the barrel to the nozzle via a three-section screw which makes the polymer granules heat into a viscoelastic melt [24]. The trapped air between the granules is expelled by virtue of the pressure developed by the screw geometry [25]. It also helps to overcome the back pressure induced by the nozzle geometry [26]. The design also comprises a heating and cooling system, a driving motor, temperature sensors, and encoders [23].

2.1. Mechanical design of the screw and selection

The screw is a very important component of the extrusion system and is often referred as the heart of the extruder [27]. The geometry of the screw is very critical in terms of the efficiency of the entire extrusion system [27]. The parameters involved in a screw geometry are channel depth, channel width, pitch, helix angle, etc. Varying any of these parameters can change the physical properties of the screw. Figure 1 shows the various components of screw geometry.

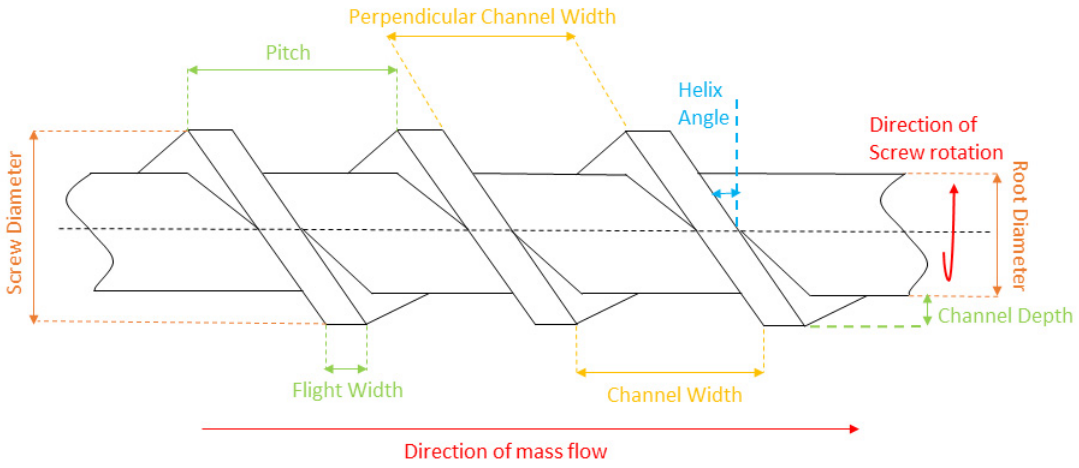

Figure 1. Components of Screw Geometry (adapted from [28]).

The screw length (L) and diameter (D) are two other important parameters of a screw extrusion system. Some studies have shown that the L/D ratio should be less than or equal to 20 for melt extruders for an efficient extrusion [29]. Table 1 shows the standard values of different screw parameters.

Table 1. Screw parameters [29].

Screw parameters	Standard values (from literature)
Length to diameter ratio (L/D)	20 or less for melt extruders
Diameter (D)	20, 25, 30, 35, 40, 50, 60, 90, 120, 150, 200, 250, 300, 350, 400, 450, 500 and 600 mm
Helix angle (ϕ)	17.65° or 0.308 rad, for $0.8 < L_S/D < 1.2$ (where L_S is pitch length)
Channel depth (h) in metering section	0.05D–0.07D for D < 30 mm, 0.02D–0.05D for D > 30 mm
Clearance between screw and barrel (δ)	0.1 mm for D < 30 mm, 0.15 mm for D > 30 mm

To minimize the gravity induced deflections in the shaft, the screw is placed in a vertical position. On the other hand, to reduce the lateral deflections, the rotation speed of the screws is intended to be low. The symmetrical sustentation provided by the molten polymers too helps in reducing the lateral deflections [30]. Inside the screw geometry, the transportation of material takes place through conveying elements. These elements have a varying pitch, which leads to the required flow compression [30]. Figure 2 shows the sectional view of the screw and the barrel arrangement used in this work.

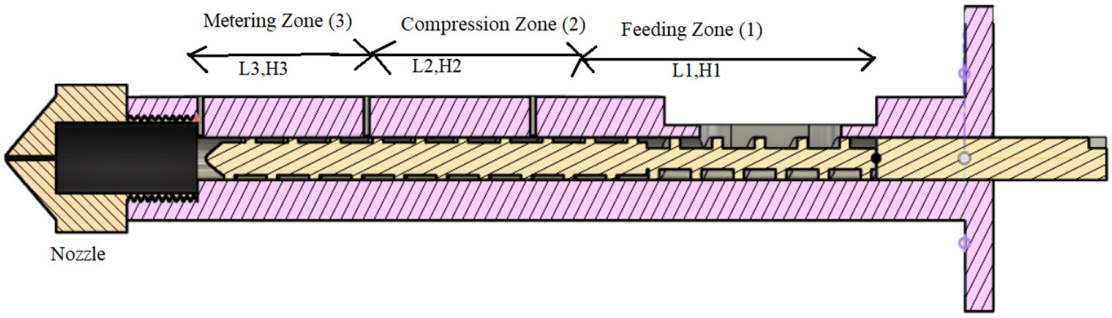

Figure 2. Sectional view of the barrel and screw arrangement.

The screw has a diameter of 11.75 mm, whereas the barrel has an inner diameter of 11.8 mm, leaving a small clearance of 0.025 mm in between. Table 2 shows all the remaining dimensions of the screw used in this work. The nozzle has a diameter of 1.75 mm. The screw, barrel, and nozzle are made of stainless steel and hence have good corrosion resistance and long service life.

Table 2. Screw geometry dimensions.

S.No.	Screw geometry parameter	Value
1	Channel width (W)	9.5 mm
2	Channel depth (H)	H1 = 3.5 mm, H2 = 3 mm, H3 = 2 mm, H = $H_{avg.}$ = 2.83 mm
3	Diameter of screw (D_s)	11.75 mm
4	Inner diameter of barrel (D)	11.80 mm
5	Outer diameter of barrel (Do)	35.60 mm
6	Thickness of barrel (t)	11.90 mm
7	Clearance between screw and barrel	0.025 mm
8	Helix angle of screw (ϕ)	0.359 rad
9	Length of the screw (L)	L1 = 65 mm, L2 = 65 mm, L3 = 60 mm, L = 190 mm

Some studies have shown that irrespective of the L/D ratio, the length of the feed zone should be constant throughout, and the remainder of the length should be dedicatedly used for melting and pumping [31]. While more channel depth results in higher specific output (lb/rpm), a larger length of the screw is taken into account in order to create the pressure required to push out the polymer from the nozzle [32]. This excessive length for the overall processing situation limits the output of the system [33]. It results in excessive melt temperature, which leads to color shift, polymer degradation, loss of adhesiveness, etc., [34]. Also, the length of the melting zone should be less if the polymer melts easily [35]. Excessive length can compromise the melting rate [36]. Lastly, for the metering zone, the length can be reduced on using proper melt pumps which can withstand the discharge pressure [32].

To increase the output, the L/D ratio can be increased [37]. However, the feed section is able to deliver polymer only up to a certain quantity limit which in turn limits the increment of ratio L/D [38]. For screws having a smaller diameter, this limit is determined by the screw strength [39]. The channel depth can be increased up to a point where the screw can bear the torque generated from the rotation [40]. On the other hand, for larger extruders, the channel depth can be increased till there is an increment in the output [41]. Increasing the channel depth beyond this point often reduces the

efficiency of feeding [42]. Hence, the L/D ratio is an important parameter as larger values of it may penalize the overall performance of the system [33].

To create an internal pressure to extrude the material, the material is compressed along the length of the screw [43]. This compression is possible due to the linearly increasing core diameter of the screw [44]. A stepper motor is used to rotate the screw in small increments to impart constant mass flow for a smooth printing process [45]. Also, to prevent any damage due to the misalignment of the screw and barrel, the latter is made from harder steel than the former [13].

Another important aspect is the size of the extruder. For higher throughput, which is also one of the objectives of this work, often larger extruders are preferred. However, at the same time, it should also be noted that while an oversized extruder provides the flexibility of having a higher output, it also results in higher daily operating costs [46]. The capital investment can increase up to double on moving up one extruder size [47]. Large extruders have more residence time for a specific output, increasing the chance of polymer degradation [48]. Additionally, the heat-up and temperature requirements are proportional to the mass of the extruder [47]. The time required for heating the extruder can double on increasing one size of the extruder [47].

Even at low speed, the AC and DC drives extract high power per unit mass of the output [49]. Due to poor power factors at low speed, DC drives are costlier than AC drives [50]. The large surface area of a big-sized heated extruder also results in increased thermal losses to the environment, which may be beneficial in cold weather but significantly increases the cost in warm weather [47]. This was the motivation for going with a small-sized extruder. Figure 3 shows the extruder assembly consisting of the screw, barrel, and the nozzle.

Figure 3. Screw extruder assembly.

Yet another important component of the screw extruder assembly is the nozzle as it is responsible for shaping the output of the polymer as well as generating pressure inside the extruder [51]. It was also observed that the smaller the nozzle size, the more pressure is required by the screw to extrude the material [52]. The end barrel section implements a detachable nozzle tip configuration with diameters ranging from 1.75 to 2.5 mm. Typical FDM systems can deposit layers within the range of 0.4 mm up to 0.8 mm thickness [53], whereas the system designed can reach up to 2 mm thickness deposition layer, which makes the system able to print higher throughputs that reduce printing time and

consequently increase the efficiency of the printing process. However, the use of the 2.5 mm nozzle resulted in unstable prints due to die-swelling issues during extrusion, which has been discussed in Section 5.1. Hence, a 1.75 mm nozzle has been used in this work throughout. On the other hand, a 1.4 mm nozzle has been used for the FDM system.

2.2. Hopper design

Since the material is gravity assisted, it becomes important to design the hopper in such a way that there is precise control of the material feed rate to avoid jamming, possibly leading to inconsistencies in print [52]. Figure 4 shows the design and the machined hopper used in this work.

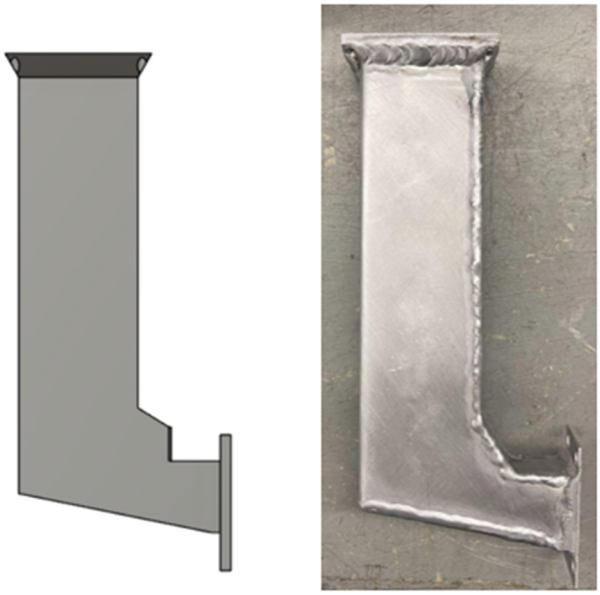

Figure 4. Hopper design and machined part.

A concerning issue in the hopper system is the agglomeration of the material near the screw-hopper assembly [54]. As the screw passes through the center of the barrel, the pellets or shredded pieces in large numbers present inside the hopper act like a barrier to the rising heat and do not allow it to escape, resulting in the heat absorption by pellets and forming agglomerates [55] as shown in Figure 5. These large groups can stall the screw and prevent the downward movement of material, eventually starving the extruder. To transport the pellets at a fixed rate, an auger screw can also be used inside the hopper [52].

Figure 5. Agglomerates of PLA pellets.

2.3. Thermal band heaters and sensors

To get the screw filled with melted polymer at an initial stage, it is important to heat the barrel to obtain a temperature suitable for the polymer to stick to the surface [56]. The angle of the screw flights then pushes the polymer forward. After the barrel heating, the energy provided to the polymer comes entirely from the screw rotation relative to the barrel, which leads to the polymer's melting by shear [57]. The polymer inside the extruder gets heated to a viscoelastic melt when subjected to shear forces. The trapped air between the melted polymer is expelled by virtue of the pressure developed by the screw geometry [58]. It also helps to overcome the back pressure induced by the nozzle geometry [24]. The screw rotation speed and the object thickness directly affect the shear rate [59]. Hence polymers experience zero shears at the screw root and maximum shear at the barrel surface. The compression section of a screw comprises a gradually reducing channel depth which forces any unmelted polymer towards the barrel wall to impart maximum shear [60].

Out of the many ways of supplying heat, an electric band heater is used in this work as it was easy to use and made it possible to control the heat characteristics. The temperature of the heaters was controlled using temperature sensors. Four band heaters have been used in the system. These band heaters have a power of 225 W operating at 120 V, a maximum heat output of 350 °C, and have been placed at various locations at the barrel surface. A PT1000 temperature sensor has been installed for each of the heaters to control their temperature individually if required. It can measure temperature up to 400 °C. Figure 6 shows the arrangement of the heaters as well as the temperature sensor.

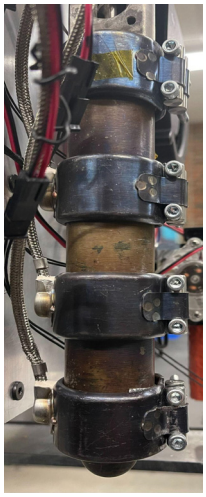

Figure 6. Arrangement of band heaters and thermistor.

Although heating is an important and essential aspect of the extrusion process, there is a possibility of an upward flow of heat through the screw and the hopper, which can be detrimental as it can lead to the partial melting of the material and convert them into agglomerates [55]. Hence, to prevent this backward flow of heat, a cooling system must be installed close to the neck of the extruder [52]. Hence the current design consists of a cooling fan installed at the junction of the hopper and the barrel of the extruder, as shown in Figure 7.

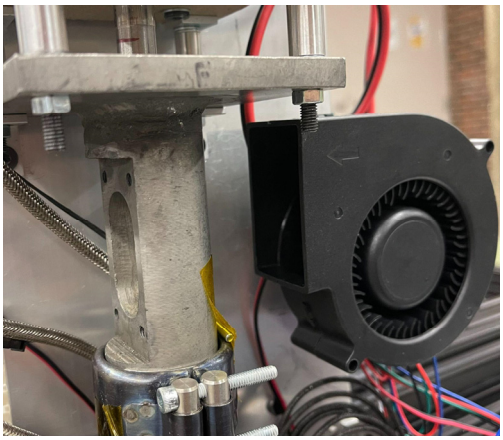

Figure 7. Cooling fan to control backflow of heat.

Lastly, to improve the thermal insulation of the extruder in order to avoid the premature melting of the small-sized particles [11], the walls of the barrel are insulated with mineral wool, as shown in Figure 8.

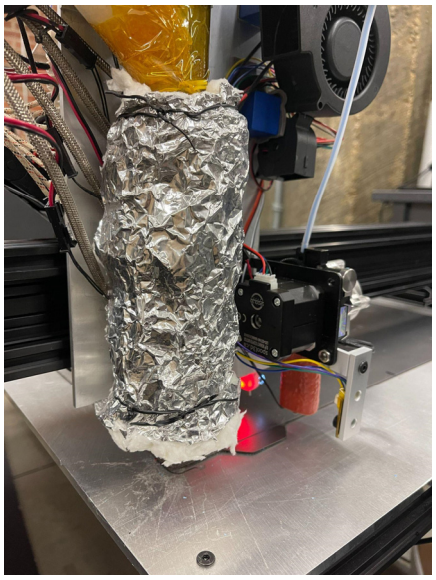

Figure 8. Mineral wool applied on barrel wall for thermal insulation.

2.4. Stepper motor and encoder

Apart from the screw geometry, the rotation of the screw is another important aspect of a screw extrusion system. The rotation of the screw pressurizes the plastic, due to which it moves and gains the heat from the barrel under friction [61]. An appropriate amount of power is needed to rotate the screw to carry on the screw extrusion mechanism. This power required is dependent on many factors, and the calculation for power requirement has been discussed in Section 3.3. As for the case of the direct fused deposition element, the target to reach 5 mm^3/s as a maximum flow rate serves as the baseline to select the electric engine which can push the melted material at a continuous rate. The dependency of the volumetric flow rate of plastics on the screw rotation speed is shown in Section 3.2.

A large fraction of the drive power (almost 85%) is used for the screw rotation, and the remaining power is used for mixing, pressurizing, and forwarding the melted polymer [62]. During the screw rotation process, the barrel heaters are in a cooling mode for a large duration and have almost no contribution to melting the polymers [63]. However, the initial barrel heating decreases the power requirement from the drive [64]. The viscosity of the polymer during shearing is directly related to the energy imparted by the screw drive [65]. As preheated polymers have less viscosity, less power is required for melting and remainder processes [62].

In the current design, a closed loop NEMA 23-sized stepper servo motor has been used. It has a 1.8-degree step angle, up to 3 N-m holding torque, and maximum current consumption of 4 A and operates at a DC voltage of 24–50 V [66]. Hence, the maximum power output is around 200 Watts. It has a built-in encoder having a high resolution of 4000 pulses per revolution. The encoder ensures high precision and no loss of step. In addition, the motor also has a stepper driver with a maximum step count of 40000 steps and 16 types of micro steps, which allows accurate functioning of encoder feedback. The motor shaft has a diameter of 8 mm; hence, an 8 × 12 mm coupler has been used to connect the motor and the screw. Figure 9 shows the NEMA 23 motor, inbuilt encoder, and the motor driver.

Figure 9. Closed loop servo motor with encoder and drivers.

2.5. Controlling systems

While the screw-extruding configuration is the mechanism to melt and deposit the material, the driven force required to deposit printed layers at specifically extrusion velocity at a controlled melting temperature requires the selection of integrated sensors and control components to push, and heat and move both the FDM and DFDM systems selectively. In the current hybrid system, it is essential to have an appropriate controlling system to regulate all the electronic components. Hence for this purpose, a Duet 3 6HC mainboard, a Duet 3 3HC expansion board, and a Duet 3 1XD expansion board have been used to form a connection between all the entities. These boards allow customized expansion of modules and provide good flexibility for machine design. This hardware system is enabled with RepRap firmware which runs on a single board computer (SBC). The sequential arrangement of all the control boards used in the current design is shown in Figure 10.

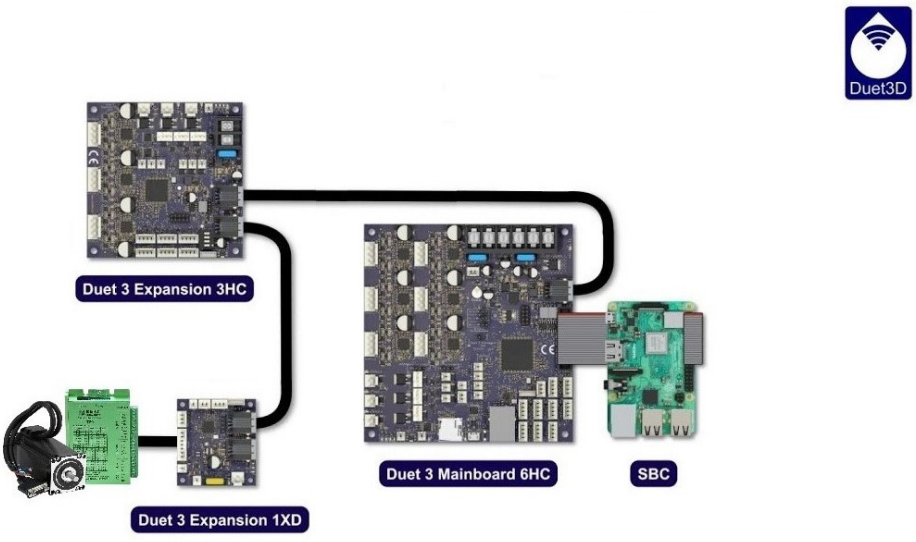

Figure 10. Sequential arrangement of control boards.

The Duet 3 6HC mainboard is a high-power controller and includes 6 high current stepper drivers, 4 high current loads, and up to 6 fans. It has the capability to add more IO channels on board through CAN-FD-connected expansion boards. In the current design, the five stepper motors (one NEMA 17 for x-direction, two NEMA 23 for y-direction, and two NEMA 23 for z-direction) for movement in the three axes, one end stop sensor each for x and y-direction, two-bed platform heaters as well as two Solid state relays for the heaters and two thermocouples are connected. The Duet 3 3HC expansion board has been connected to the 6HC mainboard with the CAN bus cable. It is a high current expansion board that contains 3 stepper drivers, 3 current loads, 6 fans, and 6 IO channels. In the current design, four band heaters (DFDM), temperature sensors for these heaters (DFDM), cooling fan (DFDM), extruder fan for the conventional FDM system, cooling fan (FDM), heater (FDM), and temperature sensor (FDM) are connected to this expansion board. Finally, the Duet 3 1XD expansion board is connected to the 3HC expansion board with the help of a CAN bus cable. This board is responsible for providing a connection to an external stepper driver and can accept up to 48 V input. In the current design, the stepper servo driver of the NEMA 23 motor (for screw rotation) is connected with this expansion board. Figure 11 shows the connections made within the Duet 3 6HC mainboard, SBC (Raspberry Pie), Duet 3 3HC, and 1XD expansion boards.

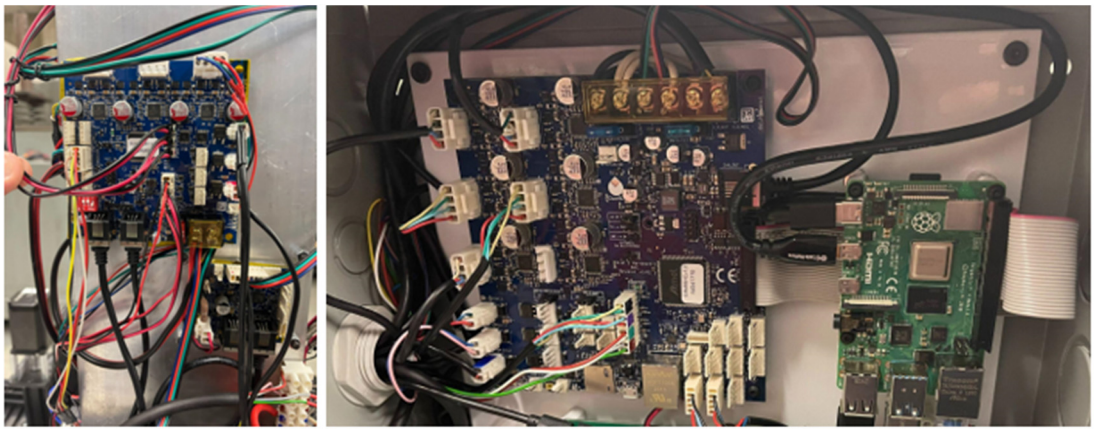

Figure 11. Connections of different control boards.

This entire hardware arrangement is controlled by RepRap Firmware (version 3.4). It is an object-oriented C++ control program for self-replicating 3D printers. The G codes are sent to the software using a Duet 3 Web interface through Wi-Fi. Figure 12 shows the Duet 3 web interface.

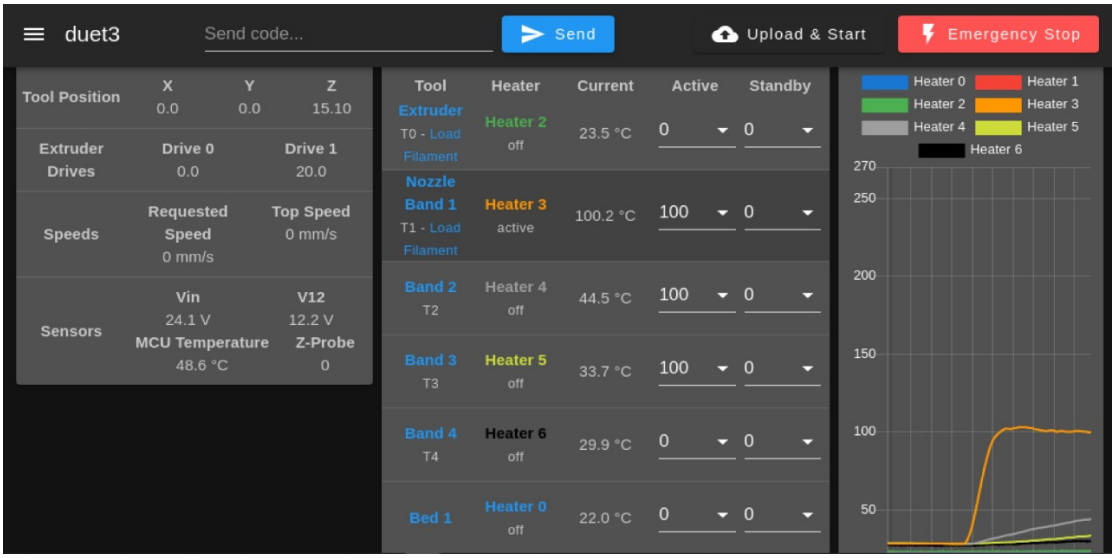

Figure 12. Duet 3 web interface.

2.6. Hybrid configuration design and assembly

One of the future objectives of this work is to print multi-material 3D objects which is possible only through the concept of hybrid 3D printing, which integrates multiple 3D printing technologies onto a single manufacturing platform. It has the combined advantages of each 3D printing technique's unique processing capability, making it feasible for many materials [67]. After completing literature surveys on various aspects of the DFDM system, the components and the complete assembly were designed on Fusion 360. The design of the system and the actual system are shown in Figures 13 and 14.

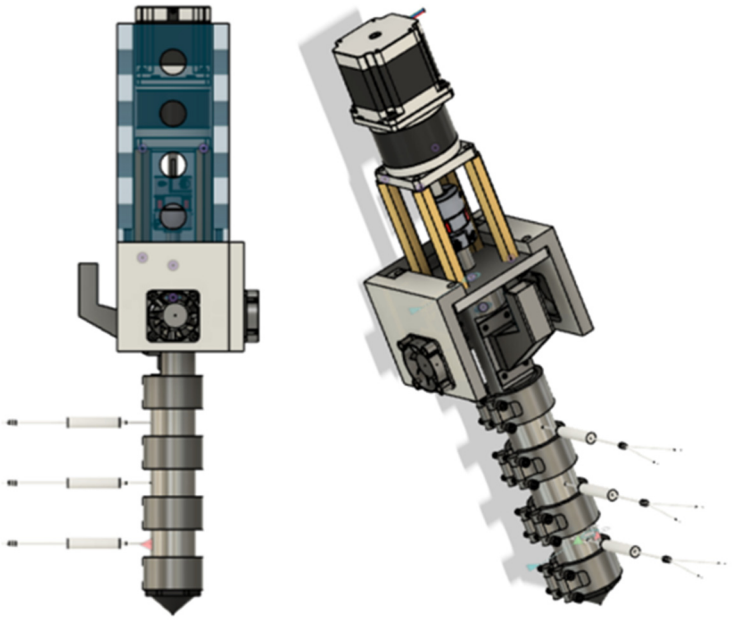

Figure 13. CAD model of DFDM system.

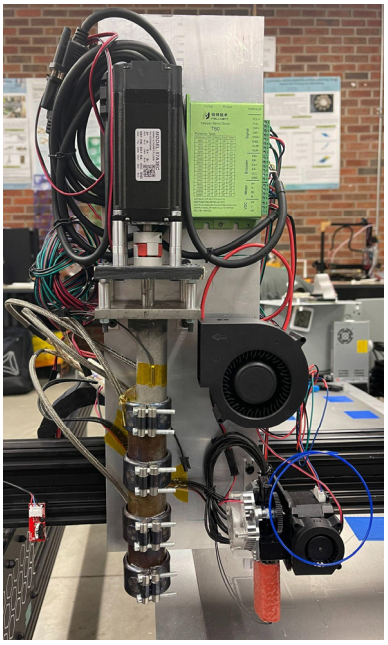

Figure 14. Hybrid system consisting of both FDM and DFDM systems.

3. Technical modeling

3.1. Barrel material selection

Any cylindrical body, such as a tube or a pipe, develops stresses at the circumference when pressure is applied [68]. To avoid bursting by virtue of pressure, these internal stresses act in the transverse direction and are tensile in nature. These are called Hoop stresses [69] and shown in Eq 1. The barrel used in the DFDM system is cylindrical, and a Hoop stress analysis has been done to analyze the material that can be used for the barrel in this work. As mentioned earlier, PLA has been used in this work, and Table 3 shows the viscosity values of PLA at different temperatures. The calculations are derived from [68,70].

$$\text{Hoop stress } (\sigma_H) = (P*d)/(2*t) \tag{1}$$

where, P = internal pressure in Pa, d = internal diameter of cylinder (here barrel) (mm) and t = wall thickness (mm). Equations 2 and 3 show the relationship between internal pressure and volumetric flow rate and dimensions of the screw and barrel geometry.

$$P = (\mu*Q)/K, \tag{2}$$

$$\text{where } K = (\pi*R^4)/8L = (\pi*D^4)/(128*L) \tag{3}$$

here, L is the length of the barrel, and μ is the viscosity of the material. Equation 4 shows the most simplified version of hoop stress required for this work.

$$P = (128*\mu*Q*L)/(\pi*D^4)$$
$$\text{Also, } d = D \text{ (barrel inner diameter)}$$
$$\sigma_H = [(128*\mu*Q*L)*(D)]/[2*t*(\pi*D^4)] = (64*\mu*Q*L)/(\pi*D^3*t) \tag{4}$$

Therefore, $\sigma_{H(max)} = (64*\mu_{(max)}*Q_{(max)}*L)/(\pi*D^3*t)$

Now, $Q_{(max)}$ = 5 mm^3/s, L = 190 mm, D = 11.8 mm, t = 11.9 mm.

Table 3. Viscosity values at different temperatures for PLA [71].

Temperature	Viscosity of PLA in Pa-s
180 ℃	3037
190 ℃	2360
200 ℃	1232
210 ℃	733

$\mu_{(max)}$ = 3037 Pa-s (at 180 ℃)

or $\mu_{(max)}$ (PLA) = 3037 N-s/m^2 = 3.037 kg/mm-s

$\sigma_{H(max)} = (64*3.037*5*190)/(\pi*11.8^3*11.9)$ = 3.008 kg/mm-s^2

$\sigma_{H(max)}$ = 3008 N/m^2, factor of safety = 5 [72]

$\sigma_{H(max)}$ = (3008*5) N/m^2 = 15040 N/m^2

Therefore, $\sigma_{H(max)}$ (PLA) = 15 kN/m^2

$\sigma_{H(max)}$ (barrel) = 15 kN/m^2 = 0.015 MPa

From calculations, it can be deduced that any material that can withstand the stresses equivalent to 0.015 MPa is an ideal material for a barrel, which is insignificant when compared to the strength of commercial metals. For the current hybrid system, a barrel made of stainless steel (tensile strength of around 600 MPa [73]) has been used to handle all the stresses generated by internal pressure.

3.2. Flow rate calculations

For initial trials, it becomes necessary to have a base value for screw rotation speed to ensure that a safe input value of rotation is fed to the control system. These calculations aim to form a relation between the screw rotation speed (N) and the volumetric flow rate (Q). A Q value of 5 mm^3/s has been targeted; accordingly, the corresponding value of N has been determined for initial trials. This relation between Q and N is based on screw extrusion theory and has been completely derived from [70] and is shown below.

From Figures 15 and 16, the down channel velocity component of the material, "V_z", can be expressed in terms of the tangential velocity "V" as shown in Eq 5:

$$V_z = V*\cos ø \tag{5}$$

Volumetric flow rate from drag (Q_D) is given as in Eq 6:

$$Q_D = W\int_0^H v(y)dy \tag{6}$$

Since the velocity profile for a Newtonian fluid is linear, $v(y) = V_z * y/H$

$$Q_D = W*(V_z/H)\int_0^H ydy$$

$$Q_D = (W*V_z*H)/2$$

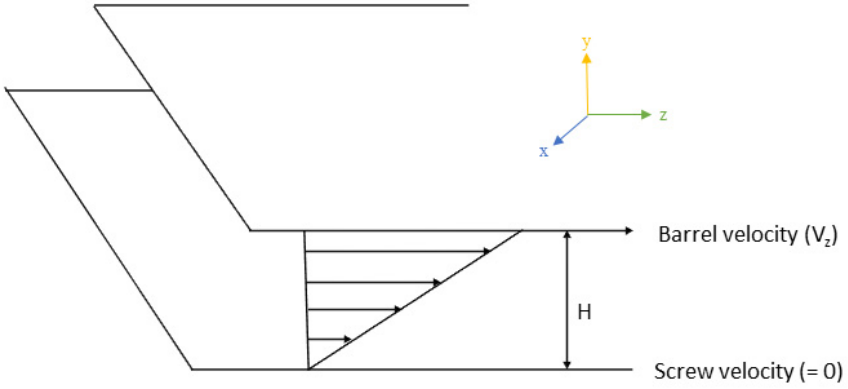

Figure 15. Drag flow mechanism (adapted from [70]).

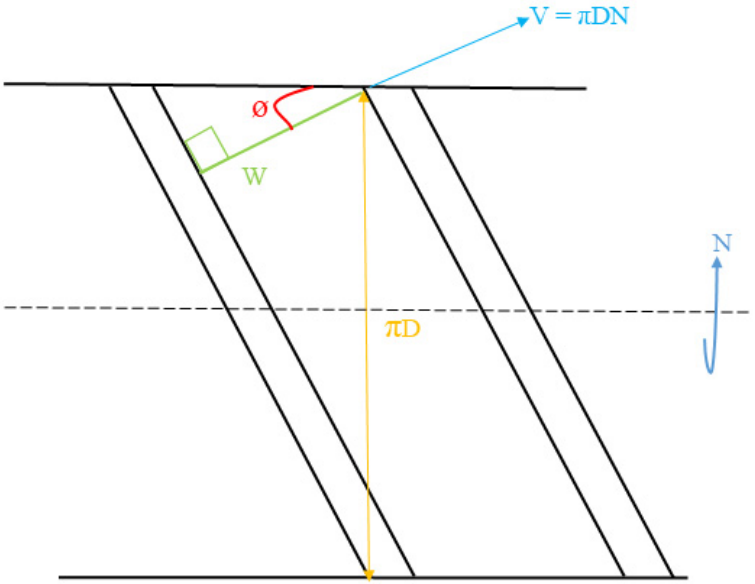

Figure 16. Unrolled single turn of the extruder screw helix (adapted from [70]).

From Figure 16, the tangential velocity at the barrel surface is related to the rotational speed of the screw and is shown in Eq 7:

$$V = \pi * D * N \tag{7}$$

Therefore, the down channel velocity component can be given as: $V_z = \pi * D * N * \cos\phi$
Hence, Q_D simplifies as shown in Eq 8:

$$Q_D = (\pi/2) * W * H * D * N * \cos\phi \tag{8}$$

An important point about the screw mechanism which needs to be considered is that the total pressure along the length of the screw is the sum of pressure changes across all the three zones which can be described by: Back pressure (ΔP) = $\Delta P_{feed.} + \Delta P_{comp.} + \Delta P_{meter.}$ [52]. This back pressure creates

some flow restrictions that works against the flow through the screw. This volumetric flow rate by virtue of the back pressure generated is shown in Eq 9:

$$Q_P = -(W/12)*H^3*(\Delta P/\mu*L) \quad (9)$$

The net volumetric flow rate is the sum of Q_D and Q_P, and is derived below in Eqs 10 and 11:

$$Q = Q_D + Q_P \quad (10)$$

$$Q = [(\pi/2)*W*H*D*N*\cos\phi] + [-(W/12)*H^3*(\Delta P/\mu*L)]$$

The net volumetric flow rate (Q) and pressure drop (ΔP) can be related as:

$Q = (K*\Delta P)/\mu$, where $K = (\pi*R^4)/8L$ {for a circular die according to Hagen–Poiseuille Law}

Here μ is the viscosity of the material present in the system, which is PLA in this work.

$$\Delta P = (\mu*Q)/K, \text{ where } K = (\pi*R^4)/8L = (\pi*D^4)/(128*L)$$
$$\Delta P = (128*\mu*Q*L)/(\pi*D^4)$$
$$(\Delta P/\ \mu*L) = (128*Q)/(\pi*D^4)$$
$$Q = [(\pi/2)*W*H*D*N*\cos\phi] + [-(W/12)*H^3*(128*Q)/(\pi*D^4)]$$
$$Q\,[1 + (W/12)*H^3*(128*Q)/(\pi*D^4)] = (\pi/2)*W*H*D*N*\cos\phi$$
$$Q\,[(32W*H^3 + 3\pi*D^4)/(3\pi*D^4)] = (\pi/2)*W*H*D*N*\cos\phi$$
$$Q = (3\pi^2*W*H*D^5*N*\cos\phi)/(6\pi*D^4 + 64W*H^3) \text{ {here Q is in mm}}^3\text{/min}\}$$

For mm^3/s, dividing by 60 on both the sides of the equation:

$$Q = (\pi^2*W*H*D^5*N*\cos\phi)/(120\pi*D^4 + 1280W*H^3) \quad (11)$$

On substituting values of screw geometry parameters, the relation between the volumetric flow rate and screw rotation speed is found to be:

$$Q = 7.5*N,$$

where N is in rpm and Q is in mm^3/s

$$\text{Conversely, } N = 0.133*Q$$

Hence for the DFDM system in this work, the rotational speed required for a screw in rpm is mathematically 0.133 times the volumetric flow rate in mm^3/s. To get the targeted volumetric flow rate of 5 mm^3/s, the screw should have a speed of 0.67 rpm, which is quite insignificant compared to realistic values.

3.3. Power calculations

As discussed earlier, inside the extruder, the polymers are melted almost entirely by virtue of viscous dissipation due to the rotation of the screw inside the barrel. The polymer melt film adhered to the barrel surface experiences a shear force by the turning screw, which causes it to stretch [74]. The resistance offered to the screw rotation while stretching the melt film is overcome by the power provided to the screw by the extruder drive [75]. This energy from the drive increases the melt film temperature and melts any unmelted material in the vicinity by virtue of transferred heat. Different polymers have different energy requirements based on the energy requirements for reaching the processing temperature [76].

Several parameters affect the power required to melt the polymer, such as the specific heat of the polymer, output mass flow rate, and the final melt temperature. Additionally, there are several energy losses in the system due to thermal losses, driver efficiency, gearbox efficiency, and power required for melting pressurization. From studies, it has been found that around 35% of additional energy is required to compensate for these losses [77]. As per the calculations, Btu/hr should be multiplied by 1.35 and a conversion factor of 0.000393 to get the horsepower (hp) [77].

From [77], the equation for Power required to melt the polymer is given below in Eq 12.

$$\text{Power (hp)} = (0.000393*1.35)*(\dot{m}\ (\text{lb/hr}))*(\text{specific heat © (Btu/lb-°F)})*(\text{temperature rise in the barrel}) \quad (12)$$

Since the current design has been tested on PLA, the required material properties are derived from [78] and used in the equation. Also, as mentioned earlier for the case of the direct fused deposition element, the target to reach 5 mm^3/s as a maximum flow rate serves as the baseline to select the electric engine. The mass flow rate value has been found accordingly. The calculations are shown below.

$\dot{m}$ = Volumetric flow rate (= 5 mm^3/s) * Density (= $1.24*10^{-6}$ kg/mm^3) = $6.2*10^{-6}$ kg/s = 0.0492 lb/hr

Max T_{req} = 220 °C = 428 °F, T_{room} = 25 °C = 77 °F, C = 1800 J/Kg-K = 0.429922 Btu/lb-°F

P = 0.00053*0.0492*0.429922*(428-77) hp

P = $3.93*10^{-3}$ hp = 2.93 watts

A power of around 3 W is required to melt PLA and achieve a volumetric flow rate of 5 mm^3/s. The NEMA 23 stepper motor used in this work can provide up to 200 W of power output, which makes the input power requirement of 3 W quite insignificant.

4. Materials

As far as this work is concerned, the proposed hybrid system has been tested only for PLA. Multi-material printing using other potential thermoplastics such as ABS, HIPS, and PC using this hybrid system is one of the future objectives of this work. Virgin PLA pellets (grade 4043D) have been used for trials. The pellet size was in the range of 2–5 mm. For the recycling counterpart, 3D printed PLA parts were shredded using a shredder and reduced to a size ranging from 2–3 mm. Here, it is important to clarify that the shredded PLA parts were printed from virgin PLA on the FDM system of this proposed hybrid system. The parts were similar and made from the same grade of PLA throughout to avoid material contamination. Additionally, the proposed hybrid system has been tested only for one-time recycled PLA and printing with multiple times recycled materials is yet another future objective of this work.

Based on the literature survey and the trials conducted, some material properties for the current DFDM system are shown in Table 4.

Table 4. Material specifications.

Material	Material size	Standard extrusion temperature range	Standard bed temperature range	Drying temperature	Drying time
PLA (4043D)	2–5 mm	210–230 °C	60–80 °C	175 °F	4 hours

5. Experimental results

Since FDM is a conventional method, this technology's printing parameters for PLA are known. However, in the case of DFDM, print parameters were unknown and needed to be found out. For this, the pellets were loaded into the hopper, keeping the initial temperature the same as FDM. The DFDM experimental setup needed a high temperature to obtain a homogeneous melt; hence, the temperature was constantly increased by a margin of 5 °C to have stable extruding. Various trials were conducted both for virgin and recycled PLA. Parameters such as temperature, screw rotation speed, layer height and nozzle diameter were adjusted as per the results obtained from the print.

5.1. Layer deposition testing

To ensure a good value of layer height, the DFDM system was made to extrude in a linear direction. After several trials, a layer height of 1.4 mm was found to be the most optimal one as it resulted in uniform and better extrusion. Figure 17 shows the trials on layer height is done.

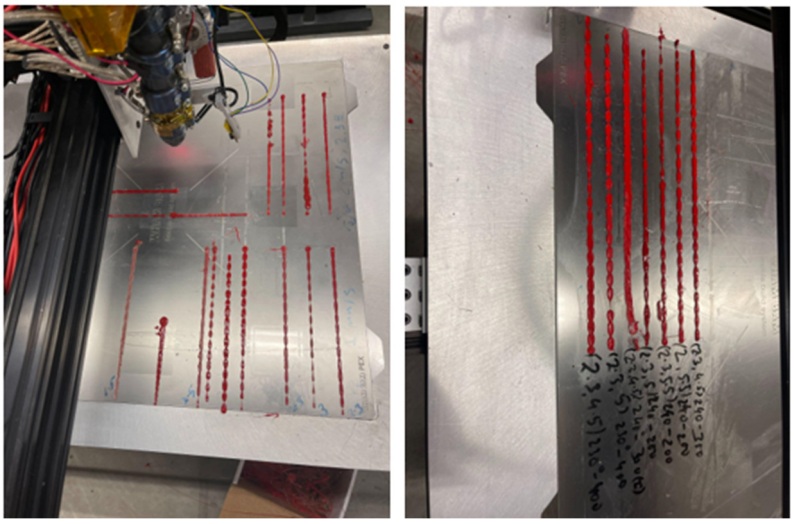

Figure 17. Layer deposition testing.

Nozzle diameter was another factor that affected the quality of the print. The use of a 2.5 mm nozzle resulted in Die-swelling issues. This is a phenomenon in which the extrudate diameter becomes larger than the channel size or the nozzle diameter [79]. This created irregularities on the walls of the print, as shown in Figure 18.

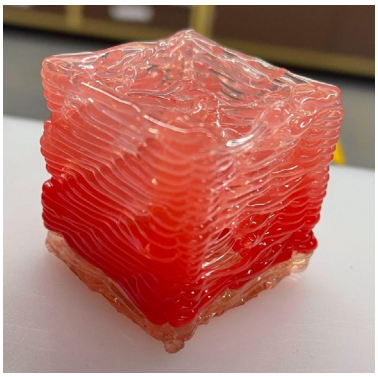

Figure 18. Irregular print due to die-swelling issue.

5.2. Printing trials

A box geometry was printed using the DFDM system using both virgin and recycled PLA, one at a time. Several print trials were done to develop optimized printing parameters for both virgin and recycled material. Figure 19 shows the DFDM system printing virgin PLA.

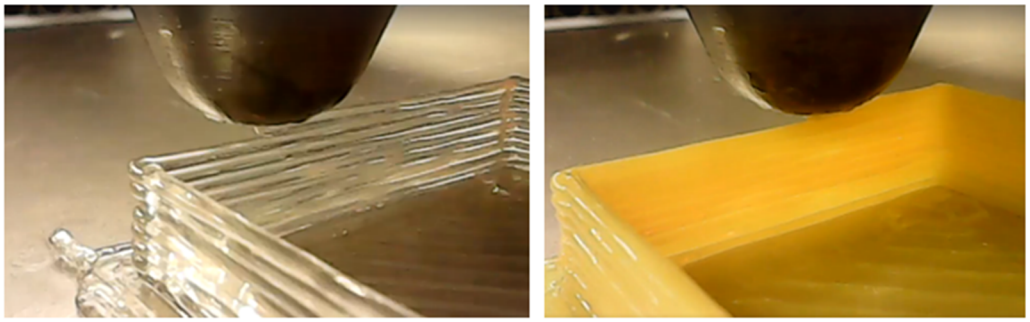

Figure 19. Printing trial with virgin PLA using DFDM system.

The print parameters for virgin PLA pellets used in the trials are shown in Table 5.

Table 5. Printing parameters for virgin PLA**.**

S.No.	Print parameter	Value
1	Screw speed	2 mm/s
2	Layer height	1.4 mm
3	Temperature profile (band heater temperatures from bottom to top)	175 ℃, 165 ℃, 155 ℃, 150 ℃
4	Bed temperature	60 ℃

Figure 20 shows some failed as well as successful trials using virgin PLA pellets.

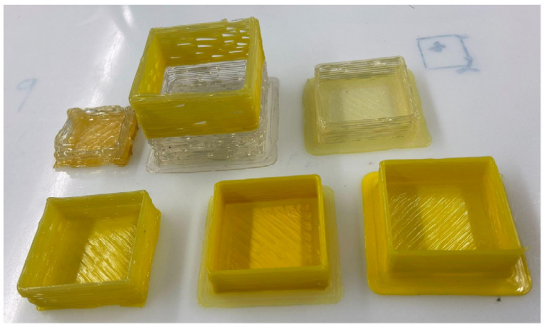

Figure 20. Print trials using virgin PLA.

Once successful printing was achieved for virgin PLA, the next target was to make sure that the system works well with recycled PLA as well. The recycled PLA material was prepared by shredding the parts printed from the FDM setup of the hybrid system as shown in Figure 21.

Figure 21. FDM printing of PLA parts.

For this, the trials were initiated with the same printing parameters as used for virgin PLA. Although, some parameters such as screw speed and temperature were continuously changed to come up with an optimized set of parameters. The main challenge was the non-uniform size of the shredded PLA particles as shown in Figure 22.

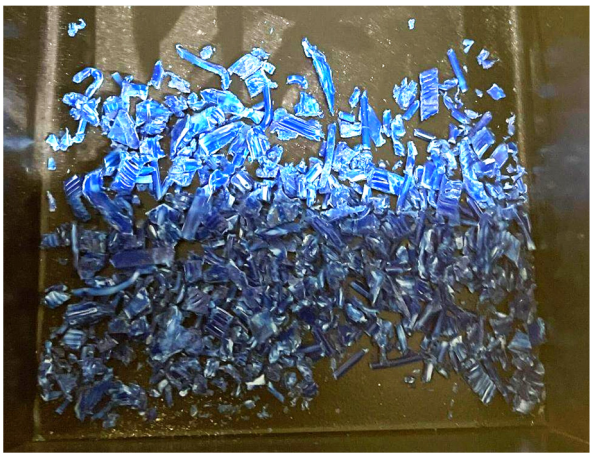

Figure 22. Shredded PLA particles (recycled).

After several trials, it was concluded that particle size within the range of 2–4 mm suits the best for this system. Figure 23 shows many failed prints using recycled PLA before reaching the most optimized print. Since the scope of this work was just to design the system and not to come out with the most optimized set of parameters, there is a huge scope for improving the quality of the prints, which is also one of the future objectives of this work.

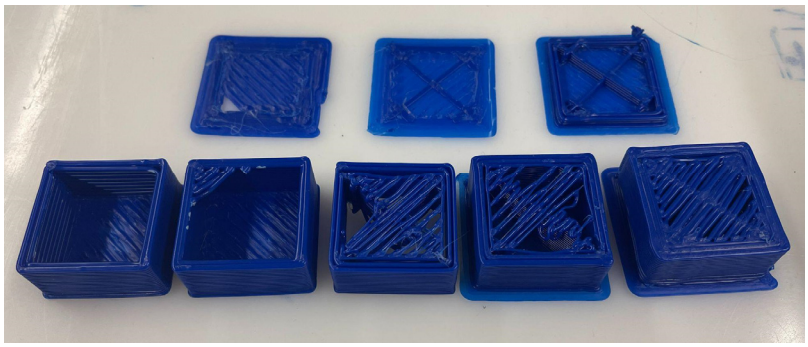

Figure 23. Print trials using recycled PLA.

6. Applications

The market application for this system is plastic, eco-friendly 3D printing products, and the main customers' target for these systems can be categorized into two segments. The first is related to On-Demand Manufacturing Companies (ODM), specifically 3D Printing Farms, and the second is Prototyping Services Companies. Typically, these enterprises produce low-batch customized components or prototypes from commercial chains such as retail, automotive, aeronautic, aerospace, and medical [80]. Up to date, it is documented that a typical 3D printing system can produce a maximum of 30% waste from production, and prototype iterations can take up to 5000 trials before the final product launch [81]. Therefore, the proposed system aims to open a business opportunity to reuse the plastic waste generated and increase cash flow by creating cheaper and more rapid second-life products and increasing profit by reducing waste disposal costs. In Canada, there are already 80 companies that provide this production services, accounting for 3% of the global market, while the USA is the largest by region with an approximate 40% of the entire market [82].

In terms of remarkable product applications using recycled plastic within additive manufacturing, there are several examples, such as the case of the German automaker Audi [83], which now has a 3D printing factory assembly aids from its used packaging materials, as shown in Figure 24. Other companies such as Coca-Cola are printing urban furniture from plastic bottle waste, and the US carmaker Ford is producing interior car components from leftover polymer powder from its 3D printing processes and combining it with 3D printed plastic dental molds from the SmileDirect company to create plastic parts for its Super Duty F-250 truck [84]. Other cases can also be found in the furniture and decorative home applications, such as beach furniture in Greece [83] and public benches in Amsterdam that were 3D printed from local waste plastic [83].

Figure 24. A technician at Audi holds up a manufacturing tool and the plastic packing waste it was 3D printed from [83].

7. Conclusions

The main emphasis of this work was to print using a high throughput hybrid system. For this, an existing FDM system was modified, and a DFDM system was installed alongside it. This DFDM system was designed after doing an intense literature survey on various aspects such as screw geometry, thermal requirement, electrical power requirement, and sensor analysis. A CAD file for the entire DFDM system was created first to visualize the system before machining the parts. The components were assembled mechanically, keeping in mind the electronics aspect as well. Calculations were done to ensure the right material for the barrel is being used, which can handle the hoop stresses generated on the inner walls of the barrel by virtue of the internal pressure created during the extrusion process. Further calculations were done to check the power requirements to melt the PLA in the proposed system having defined screw geometries. Apart from this, a relation between volumetric flow rate and screw rotation speed was also established. The aim of this relation was to analyze the initial speed requirements to get a targeted flow rate of $5mm^3/s$. Finally, after all the electrical connections were made, the hybrid system was ready for trial. First, virgin PLA pellets ranging from 2–5 mm were tried, and based on trials, the printing parameters such as layer height, band heater temperatures, screw speed, etc., were continuously changed as per the requirement. These trials were conducted till good, and stable print was obtained. Like virgin PLA, the trials were conducted for recycled shredded PLA material till a stable print was obtained.

Acknowledgments

The authors acknowledge the financial support of this work by the Natural Sciences and Engineering Research Council of Canada (Grant No. NSERC ALLRP 561048-20 Ahmad) and Alberta Innovates (Grant No. AB Innovat ADVANCE 202102739A) for funding this project. The authors also express their sincere gratitude towards all the team members of the Laboratory of

Intelligent Manufacturing, Design, and Automation (LIMDA) group for sharing their thoughts and wisdom during the research.

Conflict of interest

The authors declare no conflict of interest.

References

1. van Giezen A, Wiegmans B (2020) Spoilt-Ocean Cleanup: Alternative logistics chains to accommodate plastic waste recycling: An economic evaluation. *Transp Res Interdiscip Perspect* 5: 100115. https://doi.org/10.1016/j.trip.2020.100115
2. Nikiema J, Asiedu Z (2022) A review of the cost and effectiveness of solutions to address plastic pollution. *Environ Sci Pollut R* 29: 24547–24573. https://doi.org/10.1007/s11356-021-18038-5
3. Stefaniak AB, Bowers LN, Cottrell G, et al. (2022) Towards sustainable additive manufacturing: The need for awareness of particle and vapor releases during polymer recycling, making filament, and fused filament fabrication 3-D printing. *Resour Conserv Recycl* 176: 105911. https://doi.org/10.1016/j.resconrec.2021.105911
4. Zander NE (2019) Recycled polymer feedstocks for material extrusion additive manufacturing, In: Seppala EJ, Kotula AP, Snyder CR, *Polymer-Based Additive Manufacturing*: *Recent Developments*, Washington DC: ACS Publications, 37–51. https://doi.org/10.1021/bk-2019-1315.ch003
5. Rosli NA, Ahmad I (2021) Mechanical properties of recycled plastics, *Recent Developments in Plastic Recycling*, Singapore: Springer, 239–258. https://doi.org/10.1007/978-981-16-3627-1_11
6. Kuclourya T, Monroy R, Cuan-Urquizo E, et al. (2022) Scientometric analysis and critical review of fused deposition modeling in the plastic recycling context. *Clean Waste Syst* 2: 100008. https://doi.org/10.1016/j.clwas.2022.100008
7. Garcia JM, Robertson ML (2017) The future of plastics recycling. *Science* 358: 870–872. https://doi.org/10.1126/science.aaq0324
8. Attaran M (2017) The rise of 3-D printing: The advantages of additive manufacturing over traditional manufacturing. *Bus Horiz* 60: 677–688. https://doi.org/10.1016/j.bushor.2017.05.011
9. Lemu HG (2012) Study of capabilities and limitations of 3D printing technology. *AIP Conf Proc* 1431: 857–865. https://doi.org/10.1063/1.4707644
10. Fenollosa F, Uceda R, Tejo A, et al. (2021) Research on desktop 3D Printing Multi-Material New Concepts. *IOP Conf Ser Mater Sci Eng* 1193: 012043. https://doi.org/10.1088/1757-899X/1193/1/012043
11. Netto JMJ, Idogava HT, Santos LEF, et al. (2021) Screw-assisted 3D printing with granulated materials: A systematic review. *Int J Adv Manuf Tech* 115: 2711–2727. https://doi.org/10.1007/s00170-021-07365-z
12. Netto JMJ, Silveira ZC (2018) Design of an innovative three-dimensional print head based on twin-screw extrusion. *J Mech Design* 140: 125002. https://doi.org/10.1115/1.4041175
13. Feuerbach T, Thommes M (2021) Design and characterization of a screw extrusion hot-end for fused deposition modeling. *Molecules* 26: 590. https://doi.org/10.3390/molecules26030590

14. Johann KS, Reißing A, Bonten C (2022) Comparative analysis of the solid conveying of regrind, virgin and powdery polyolefins in single-screw extrusion. *J Manuf Mater Process* 6: 56. https://doi.org/10.3390/jmmp6030056
15. Khondoker MAH, Sameoto D (2019) Direct coupling of fixed screw extruders using flexible heated hoses for FDM printing of extremely soft thermoplastic elastomers. *Prog Addit Manuf* 4: 197–209. https://doi.org/10.1007/s40964-019-00088-4
16. Alexandre A, Sanchez FAC, Boudaoud H, et al. (2020) Mechanical properties of direct waste printing of polylactic acid with universal pellets extruder: comparison to fused filament fabrication on open-source desktop three-dimensional printers. *3D Print Addit Manuf* 7: 237–247. https://doi.org/10.1089/3dp.2019.0195
17. Kumar N, Jain PK, Tandon P, et al. (2018) Extrusion-based additive manufacturing process for producing flexible parts. *J Braz Soc Mech Sci Eng* 40: 1–12. https://doi.org/10.1007/s40430-018-1068-x
18. Reddy BV, Reddy NV, Ghosh A (2007) Fused deposition modelling using direct extrusion. *Virtual Phys Prototyp* 2: 51–60. https://doi.org/10.1080/17452750701336486
19. Leng J, Wu J, Chen N, et al. (2019) The development of a conical screw-based extrusion deposition system and its application in fused deposition modeling with thermoplastic polyurethane. *Rapid Prototyp J* 26: 409–417. https://doi.org/10.1108/RPJ-05-2019-0139
20. Canessa E, Baruzzo M, Fonda C (2017) Study of Moineau-based pumps for the volumetric extrusion of pellets. *Addit Manuf* 17: 143–150. https://doi.org/10.1016/j.addma.2017.08.015
21. Magnoni P, Rebaioli L, Fassi I, et al. (2017) Robotic AM system for plastic materials: tuning and on-line adjustment of process parameters. *Procedia Manuf* 11: 346–354. https://doi.org/10.1016/j.promfg.2017.07.117
22. Woern AL, Byard DJ, Oakley RB, et al. (2018) Fused particle fabrication 3-D printing: Recycled materials' optimization and mechanical properties. *Materials* 11: 1413. https://doi.org/10.3390/ma11081413
23. Whyman S, Arif KM, Potgieter J (2018) Design and development of an extrusion system for 3D printing biopolymer pellets. *Int J Adv Manuf Technol* 96: 3417–3428. https://doi.org/10.1007/s00170-018-1843-y
24. Valkenaers H, Vogeler F, Ferraris E, et al. (2013) A novel approach to additive manufacturing: screw extrusion 3D-printing. *Proceedings of the 10th International Conference on Multi-Material Micro Manufacture*, Singapore, 235–238. https://doi.org/10.3850/978-981-07-7247-5-359
25. Bellini A, Güçeri S, Bertoldi M (2004) Liquefier dynamics in fused deposition. *J Manuf Sci Eng* 126: 237–246. https://doi.org/10.1115/1.1688377
26. Chiruvella RV, Jaluria Y, Sernas V, et al. (1996) Extrusion of non-Newtonian fluids in a single-screw extruder with pressure back flow. *Polym Eng Sci* 36: 358–367. https://doi.org/10.1002/pen.10422
27. Eslami H, Understanding screw design for film extrusion process. Macro Engineering and Technology, 2014. Available from: http://www.macroeng.com/understanding-screw-design-for-film-extrusion-process.php.
28. Pitayachaval P, Watcharamaisakul P (2019) A review of a machine design of chocolate extrusion based co-rotating twin screw extruder. *IOP Conf Ser Mater Sci Eng* 703: 012012. https://doi.org/10.1088/1757-899X/703/1/012012

29. Osswald TA (2017) *Understanding Polymer Processing*, 2Eds., München: Hanser. https://doi.org/10.3139/9781569906484.fm
30. Netto JMJ, Silveira ZC (2018) Design of an innovative three-dimensional print head based on twin-screw extrusion. *J Mech Design* 140: 125002. https://doi.org/10.1115/1.4041175
31. Sikora JW, Samujlo B, Stasiek A, et al. (2015) The mechanical properties of plasticized PVC processed in an extruder with a modified feed zone. *Int Polym Proc* 30: 359–365. https://doi.org/10.3139/217.3040
32. Bereaux Y, Charmeau JY, Moguedet M (2009) A simple model of throughput and pressure development for single screw. *J Mater Process Tech* 209: 611–618. https://doi.org/10.1016/j.jmatprotec.2008.02.070
33. Frankland J, Extrusion: How much L/D do you really need? Plastics Technology, 2011. Available from: https://www.ptonline.com/articles/how-much-ld-do-you-really-need.
34. Garcia D, Balart R, Sánchez L, et al. (2007) Compatibility of recycled PVC/ABS blends. Effect of previous degradation. *Polym Eng Sci* 47: 789–796. https://doi.org/10.1002/pen.20755
35. Housz JFI, Meijer HEH (1981) The melting performance of single screw extruders. *Polym Eng Sci* 21: 352–359. https://doi.org/10.1002/pen.760210606
36. Mount EM (2017) Extrusion processes, *Applied Plastics Engineering Handbook*, Norwich: William Andrew Publishing, 217–264. https://doi.org/10.1016/B978-0-323-39040-8.00012-2
37. Shankar TJ, Sokhansanj S, Bandyopadhyay S, et al. (2010) A case study on optimization of biomass flow during single-screw extrusion cooking using genetic algorithm (GA) and response surface method (RSM). *Food Bioproc Tech* 3: 498–510. https://doi.org/10.1007/s11947-008-0172-9
38. Sokhey AS, Ali Y, Hanna MA (1997) Effects of die dimensions on extruder performance. *J Food Eng* 31: 251–261. https://doi.org/10.1016/S0260-8774(96)00025-8
39. Sikora JW, Sasimowski E (2005) Influence of the length of the plasticating system on selected characteristics of an autothermal extrusion process. *Adv Polym Tech* 24: 21–28. https://doi.org/10.1002/adv.20021
40. Chevanan N, Rosentrater KA, Muthukumarappan K (2010) Effects of processing conditions on single screw extrusion of feed ingredients containing DDGS. *Food Bioproc Tech* 3: 111–120. https://doi.org/10.1007/s11947-008-0065-y
41. Vincelette AR, Guerrero CS, Carreau PJ, et al. (1989) A model for single-screw plasticating extruders. *Int Polym Proc* 4: 232–241. https://doi.org/10.3139/217.890232
42. Rauwendaal C (2004) Finite element studies of flow and temperature evolution in single screw extruders. *Plast Rubber Compos* 33: 390–396. https://doi.org/10.1179/174328904X24880
43. Chiruvella RV, Jaluria Y, Karwe MV (1996) Numerical simulation of the extrusion process for food materials in a single-screw extruder. *J Food Eng* 30: 449–467. https://doi.org/10.1016/S0260-8774(96)00022-2
44. Roland W, Marschik C, Krieger M, et al. (2019) Symbolic regression models for predicting viscous dissipation of three-dimensional non-Newtonian flows in single-screw extruders. *J Non-Newton Fluid* 268: 12–29. https://doi.org/10.1016/j.jnnfm.2019.04.006
45. Drotman D, Diagne M, Bitmead R, et al. (2016) Control-oriented energy-based modeling of a screw extruder used for 3D printing. *Proceedings of the ASME 2016 Dynamic Systems and Control Conference*, Minneapolis, USA, 12–14. https://doi.org/10.1115/DSCC2016-9651

46. Smith D, Spalding MA, Gould RJ (2008) Selecting equipment to minimize production costs and maximize profitability. *J Plast Film Sheet* 24: 21–33. https://doi.org/10.1177/8756087907087171
47. Frankland J, Get smarter on extruder sizes. Plastics Technology, 2012. Available from: https://www.ptonline.com/articles/get-smarter-on-extruder-sizes.
48. Drobny JG (2014) Thermoplastic Polyurethane Elastomers, *Handbook of Thermoplastic Elastomers*, Amsterdam: Elsevier, 233–253. https://doi.org/10.1016/B978-0-323-22136-8.00009-0
49. Abeykoon C, McMillan A, Nguyen BK (2021) Energy efficiency in extrusion-related polymer processing: A review of state of the art and potential efficiency improvements. *Renewable Sustainable Energy Rev* 147: 111219. https://doi.org/10.1016/j.rser.2021.111219
50. Berthiaume D (1991) Justification for AC vs. DC drive systems. *Conference Record of 1991 Annual Pulp and Paper Industry Technical Conference*, Montreal, Canada, IEEE, 234–238. https://doi.org/10.1109/PAPCON.1991.239643
51. Das A, Gilmer EL, Biria S, et al. (2021) Importance of polymer rheology on material extrusion additive manufacturing: Correlating process physics to print properties. *ACS Appl Polym Mater* 3: 1218–1249. https://doi.org/10.1021/acsapm.0c01228
52. Whyman S, Arif KM, Potgieter J (2018) Design and development of an extrusion system for 3D printing biopolymer pellets. *Int J Adv Manuf Technol* 96: 3417–3428. https://doi.org/10.1007/s00170-018-1843-y
53. Tian X, Liu T, Yang C, et al. (2016) Interface and performance of 3D printed continuous carbon fiber reinforced PLA composites. *Compos Part A-Appl S* 88: 198–205. https://doi.org/10.1016/j.compositesa.2016.05.032
54. Papadakis SE, Bahu RE (1992) The sticky issues of drying. *Dry Technol* 10: 817–837. https://doi.org/10.1080/07373939208916484
55. Maynard E, Mehos G, Maynard E, Handle bulk solids safely and effectively, fluids and solids handling. AIChE, 2009. Available from: https://www.aiche.org/resources/publications/cep/2009/september/handle-bulk-solids-safely-and-effectively.
56. Lipár S, Noga P, Hulkó G (2013) Modelling and control of extruder barrel temperature field. *IFAC-PapersOnLine* 46: 191–196. https://doi.org/10.3182/20130925-3-FR-4043.00078
57. La Gala A, Fiorio R, Erkoç M, et al. (2020) Theoretical evaluation of the melting efficiency for the single-screw micro-extrusion process: the case of 3D printing of ABS. *Processes* 8: 1522. https://doi.org/10.3390/pr8111522
58. Gedde UW, Hedenqvist MS, Hakkarainen M, et al. (2021) Processing of polymeric materials, *Applied Polymer Science*, Cham: Springer, 453–487. https://doi.org/10.1007/978-3-030-68472-3_8
59. Grizzuti N, Bifulco O (1997) Effects of coalescence and breakup on the steady-state morphology of an immiscible polymer blend in shear flow. *Rheol Acta* 36: 406–415. https://doi.org/10.1007/BF00396327
60. Fenner RT (1979) Introduction to the main polymer processes, *Principles of Polymer Processing*, London: Palgrave. https://doi.org/10.1007/978-1-349-16234-5
61. Rosato DV, Rosato DV, Rosato MG (2020) Plasticizing, *Injection Molding Handbook*, Boston: Springer, 151–220. https://doi.org/10.1007/978-1-4615-4597-2_3

62. Frankland J, Understanding melting in single-screw extruders. Plastics Technology, 2021. Available from: https://www.ptonline.com/articles/understanding-melting-in-single-screw-extruders-.
63. Abeykoon C, Kelly AL, Brown EC, et al. (2014) Investigation of the process energy demand in polymer extrusion: A brief review and an experimental study. *Appl Energ* 136: 726–737. https://doi.org/10.1016/j.apenergy.2014.09.024
64. Abeykoon C, Kelly AL, Brown EC, et al. (2016) The effect of materials, process settings and screw geometry on energy consumption and melt temperature in single screw extrusion. *Appl Energ* 180: 880–894. https://doi.org/10.1016/j.apenergy.2016.07.014
65. DiNunzio JC, Brough C, Hughey JR, et al. (2010) Fusion production of solid dispersions containing a heat-sensitive active ingredient by hot melt extrusion and Kinetisol® dispersing. *Eur J Pharm Biopharm* 74: 340–351. https://doi.org/10.1016/j.ejpb.2009.09.007
66. Rtelligent, T60 Closed Loop Stepper Driver User Manual, Rtelligent, n.d. Available from: http://www.rtelligent.net/upload/wenjian/Stepper/T60%20User%20Manual.pdf.
67. Zheng Y, Zhang W, Lopez DMB, et al. (2021) Scientometric analysis and systematic review of multi-material additive manufacturing of polymers. *Polymers* 13: 1957. https://doi.org/10.3390/polym13121957
68. Trenchlesspedia, Hoop Stress. Trenchlesspedia, 2021. Available from: https://www.trenchlesspedia.com/definition/2799/hoop-stress.
69. Capelle J, Dmytrakh I, Gilgert J (2006) A comparison of experimental results and computations for cracked tubes subjected to internal pressure. *Mater Tehnol* 40: 233.
70. Birley AW, Haworth B, Batchelor J, Single-screw extrusion the extruder characteristic. Deike Library, 1992. Available from: https://zeus.plmsc.psu.edu/~manias/MatSE447/21_Extrusion2.pdf.
71. Yoo HM, Jeong SY, Choi SW (2021) Analysis of the rheological property and crystallization behavior of polylactic acid (Ingeo™ Biopolymer 4032D) at different process temperatures. *e-Polymers* 21: 702–709. https://doi.org/10.1515/epoly-2021-0071
72. Engineering ToolBox, Factors of Safety. Engineering ToolBox, 2010. Available from: https://www.engineeringtoolbox.com/factors-safety-fos-d_1624.html.
73. Song R, Xiang J, Hou D (2011) Characteristics of mechanical properties and microstructure for 316L austenitic stainless steel. *J Iron Steel Res Int* 18: 53–59. https://doi.org/10.1016/S1006-706X(11)60117-9
74. Mahfuz H, Adnan A, Rangari VK, et al. (2005) Manufacturing and characterization of carbon nanotube/polyethylene composites. *Int J Nanosc*i 4: 55–72. https://doi.org/10.1142/S0219581X05002961
75. Njobet NL, Energy analysis in the extrusion of plastics. Theseus, 2012. Available from: https://www.theseus.fi/handle/10024/53774.
76. Lay M, Thajudin NLN, Hamid ZAA, et al. (2019) Comparison of physical and mechanical properties of PLA, ABS and nylon 6 fabricated using fused deposition modeling and injection molding. *Compos Part B-Eng* 176: 107341. https://doi.org/10.1016/j.compositesb.2019.107341
77. Frankland J, How much horsepower do you need? Plastics Technology, 2009. Available from: https://www.ptonline.com/articles/how-much-horsepower-do-you-need.

78. Zmeskal O, Marackova L, Lapcikova T, et al. (2020) Thermal properties of samples prepared from polylactic acid by 3D printing. *AIP Conf Proc* 2305: 020022. https://doi.org/10.1063/5.0033857
79. Liang JZ (2008) Effects of extrusion conditions on die-swell behavior of polypropylene/diatomite composite melts. *Polym Test* 27: 936–940. https://doi.org/10.1016/j.polymertesting.2008.08.001
80. Walter M, Holmström J, Yrjölä H (2004) Rapid manufacturing and its impact on supply chain management. *Proceedings of the Logistics Research Network Annual Conference*, Dublin, Ireland.
81. Kohut A, Idea Reality: Rapid prototyping and the art of failing forward. Ultimaker, 2019. Available from: https://ultimaker.com/learn/idea-reality-rapid-prototyping-art-of-failing-forward.
82. 3D.directory, 3D Printing Companies in Canada. 3D.directory, n.d. Available from: https://www.3d.directory/directory/3d-printing-services?country=Canada.
83. All3DP Pro, 3D Printing From Plastic Waste: 10 Successful Projects. All3DP Pro, n.d. Available from: https://all3dp.com/1/3d-printing-from-plastic-waste/.
84. TechSpot, Ford and HP are recycling 3D printer waste into truck parts. TechSpot, n.d. Available from: https://www.techspot.com/news/89074-ford-hp-recycling-3d-printer-waste-truck-parts.html.

AIMS Press